Heliyon 10 (2024) e41044

Contents lists available at ScienceDirect

Heliyon

journal homepage: www.cell.com/heliyon

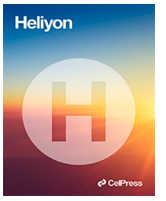

Research article

Acidic properties of propyl sulfonic acid functionalized SBA-15 catalysts for acetylation of glycerol

Panida Sriratchatchawan [a], Srisin Eaimsumang [a], Siwaporn Meejoo Smith [b], Supakorn Boonyuen [c], Chawalit Ngamcharussrivichai [d,e], Apanee Luengnaruemitchai [a,e,*]

[a] The Petroleum and Petrochemical College, Chulalongkorn University, Pathumwan, Bangkok 10330, Thailand
[b] Center of Sustainable Energy and Green Materials and Department of Chemistry, Faculty of Science, Mahidol University, Nakhon Pathom 73170, Thailand
[c] Department of Chemistry, Faculty of Science and Technology, Thammasat University-Rangsit Campus, Pathum Thani 12120, Thailand
[d] Department of Chemical Technology, Faculty of Science, Chulalongkorn University, Bangkok 10330, Thailand
[e] Center of Excellence in Catalysis for Bioenergy and Renewable Chemicals, Chulalongkorn University, Bangkok 10330, Thailand

ARTICLE INFO

Keywords:
Acetylation
Glycerol
Acetic acid
Propyl sulfonic acid
Mesoporous silica
Triacetin

ABSTRACT

Glycerol, a by-product of biodiesel production through transesterification, presents an opportunity for biodiesel industries to transform surplus glycerol into high-value chemical products. This study focuses on the development of a series of propyl sulfonic acid functionalized ($PrSO_3H$) SBA-15 catalysts, synthesized by direct synthesis of 3-mercaptopropyltrimethoxysilane (MPTMS) and tetraethoxysilane (TEOS) in an acidic medium. The catalysts were evaluated for acetylation of glycerol with acetic acid under conditions optimized through response surface methodology. Among the catalysts tested, the direct-synthesized $PrSO_3H$-SBA-15 catalyst with a 20 % MPTMS/(MPTMS + TEOS) ratio exhibited the highest amount Brønsted acid sites, resulting in a complete glycerol conversion level and 30.1 % triacetin selectivity. Notably, the catalysts maintained its conversion over three consecutive reaction runs without a significant reduction in glycerol conversion level.

1. Introduction

According to the 26th UN Climate Change Conference of the Parties (COP26) in Glasgow, the United Kingdom, the agreement for global de-carbonization was strongly emphasized. With a mission to obtain net zero carbon by 2050, more than 100 countries released their respective energy transition policy to reduce greenhouse gas (GHG) emissions by 2030 [1]. Utilization of biofuels as one of the sustainable energy sources was proposed as an effective way to reduce emissions of GHGs. The use of biodiesel has been found to reduce the emission of GHGs and particulate matter in the transportation sector and does not require any significant modification to currently used diesel engines [2].

Biodiesel can be produced using agricultural products, such as vegetable oil and animal fats, via transesterification with low molecular weight alcohols (principally methanol, ethanol, and propanol) [3]. Biodiesel is often considered as a carbon-neutral fuel because the carbon dioxide emitted during its combustion is offset by the carbon dioxide absorbed by the plants used to produce

* Corresponding author. The Petroleum and Petrochemical College, Chulalongkorn University, Pathumwan, Bangkok 10330, Thailand.
E-mail address: apanee.l@chula.ac.th (A. Luengnaruemitchai).

https://doi.org/10.1016/j.heliyon.2024.e41044
Received 29 April 2024; Received in revised form 12 November 2024; Accepted 5 December 2024
Available online 9 December 2024

biodiesel feedstock through photosynthesis. The high demand for biodiesel resources has stimulated the agricultural economy [4], but its production and consumption have also raised concerns. When derived from edible feedstocks like palm oil, soybean oil, biodiesel can drive up the price of these commodities, affecting food security. Even non-edible oil feedstocks can still compete with food crops for agricultural land. Unfortunately, a glut of crude glycerol results since this is generated at 10 % (w/w) of the total biodiesel produced. Usage of crude glycerol is very limited and so this glut has adversely affected the global market price of glycerol [5]. Therefore, the conversion of crude glycerol into valuable products is one of the attractive solutions to improve the economic viability of biodiesel manufacturing. Glycerol can be transformed into many valuable products, such as propionic acid, lactic acid, citric acid, propanediol, ethanol, etc. In the field of biofuel, the prominent glycerol derivative product is acetin, which is formed via acetylation (usually with acetic anhydride or acetic acid) [6] in the presence of an acid catalyst. Generally, acetin are composed of three structures which are mono-, di-, and tri-acetin. Monoacetin and diacetin are easily generated through acetylation reaction and can be utilized as food additive [7], plasticizer and solvent [8]. However, among three products (mono-, di-, and tri-acetin), triacetin has been used in wide range and significant applications as an additive of biodiesel fuel compositions [9].

Several heterogeneous catalysts have been used in the acetylation reaction of glycerol and acetic acid in order to promote glycerol conversion and selectivity for triacetin production since these have the advantages of the reusability and ease of separation of the catalyst from the reaction mixture. Shape selectivity, acidic property, and reusability are the main criteria for catalyst selection in the acetylation reaction, and typically include zeolite and Amberlyst resin [10] (shown in Table 1). In addition, the textural properties of the catalyst must be appropriate to the chemical reactant and products. As the acetylation reaction proceeds, the structures of all the products (mono-, di-, and tri-acetin) are marginally enlarged. The critical diameter of triacetin, the last formed and most desired product, is 1.021 nm; therefore, the pore size of the catalyst is expected to be one of the crucial parameters for this reaction.

Three zeolite H-Y, H-beta, and H-ZSM-5, with an average pore diameter (d_p) of 0.81, 0.74, and 0.62 nm, respectively, were studied in glycerol acetylation with acetic anhydride. The 100 % triacetin selectivity was obtained at reaction conditions at 80 °C, anhydride to glycerol molar ratio of 5, catalyst amount of 0.25 g (5 wt% of glycerol), no stirring by zeolite H-Y with the large pore size and less acidic, suggesting that the d_p of the catalyst can significantly affect triacetin formation [10]. In case of the propyl sulfonic acid ($PrSO_3H$)-functionalized on mesoporous silicas (SBA-15 and SBA-16) with large pore diameter of 5 and 6.5 nm, the existence of Brønsted acid sites and triacetin selectivity (21.5 %) on the $PrSO_3H$-SBA-15 was higher than on the $PrSO_3H$-SBA-16 (18.1 % triacetin selectivity) at reaction conditions of 130 °C, acetic acid to glycerol weight ratio of 5, catalyst amount of 0.05 g [11]. Likewise, commercial resin amberlyst-15, a Brønsted acid catalyst with an acidity of 4.7 mmol/g, gave a 97.1 % glycerol conversion and 19.7 % triacetin selectivity at a reaction condition of a 1:6 glycerol: acetic acid molar ratio, catalyst concentration of 5.53 g/L and stirring speed of 800 rpm and 100 °C [12]. In contrast, aluminium oxide, a Lewis acid catalyst, yielded only a 33.4 % glycerol conversion and 0.3 % triacetin selectivity at the same reaction conditions, suggesting the requirement for Brønsted acid sites [12].

Among the potential catalysts, ordered mesoporous silica SBA-15 has the advantage of having a high surface area, easy preparation, controllable structure, and ability to incorporate multi-functional groups into its channels with a one-step procedure. A comparative study of $PrSO_3H$-SBA-15 and $PrSO_3H$-silica (SiO_2) catalysts was conducted over six successive cycles [13]. The $PrSO_3H$-SBA-15 catalyst demonstrated a consistent ability to produce triacetin, attributed to its sulfonic acid groups. In contrast, severe leaching of the sulfonic acid groups from the $PrSO_3H$-SiO_2 was evidenced by the disappearance of the S 2p X-ray photoelectron spectroscopy (XPS) spectra from the catalyst surface. Although $PrSO_3H$-SBA-15 catalysts with a high acidity have received attention as potential catalysts for many

Table 1
Catalytic activities of different catalysts studied in acetylation of glycerol.

Catalyst	Glycerol (wt%)	Temp (°C)	Mole ratio Glycerol/ Acetic acid	Pore diameter (nm)	Conversion (%)	Triacetin selectivity (%)	Brønsted (mmol H^+/ g)	Lewis (mmol H^+/g)	Total[a] (mmol H^+/g)	Ref
Zeolite H-Y	5	100 (1 h)	1:5 (Ac_2O)	0.81	100	100	0.59	0.24	0.83	[10]
Zeolite H-beta	5	80 (2 h)	1:5 (Ac_2O)	0.74	100	40	0.53	0.25	0.78	[10]
Zeolite H-ZSM-5	5	80 (2 h)	1:5 (Ac_2O)	0.62	100	13	1.09	0.05	1.14	[10]
$PrSO_3H$/ SBA-15	2.5	130 (1 h)	1:5	5.1	100	21.5	n/a	n/a	0.60[b]	[11]
$PrSO_3H$/ SBA-16	2.5	130 (1 h)	1:5	6.5	52.0	18.1	n/a	n/a	0.40[b]	[11]
Amberlyst-15	5	110 (4 h)	1:6	30.0	97.1	19.7	n/a	n/a	4.7[c]	[12]
Al_2O_3	5	110 (4 h)	1:6	4.2	33.4	0.3	n/a	n/a	0.17[b]	[12]
$PrSO_3H$-SBA-15	5	105 (3 h)	1:3	9.4	100	33	n/a	n/a	1.2[b]	[13]
$PrSO_3H$-SiO_2	5	105 (3 h)	1:3	4.6	100	49	n/a	n/a	1.7[b]	[13]

[a] Measured by pyridine adsorption–desorption FT-IR for zeolites.
[b] Calculated by TPD of NH_3, total acid sites (mmol NH_3/g).
[c] Manufacturer datasheet, acidity (mmol/g).

reactions, each catalyst needs to be discussed in terms of the specific requirements for this reaction. The challenge in acetylating glycerol to triacetin using $PrSO_3H$-SBA-15 catalysts prepared by direct synthesis lies in optimizing the acidic sites on the catalyst. To understand how these acidic sites, which are critical for the reaction, relate to the catalyst's performance, we quantify their nature and distribution using pyridine-FTIR spectroscopy.

The aim of this research was to prepare the $PrSO_3H$ functionalized SBA-15 by two synthesis methods (direct and post synthesis) and investigate their performance on triacetin formation from the acetylation of glycerol. In particular, the $PrSO_3H$ functionalized SBA-15 with a high degree of Brønsted acid sites and their arrangements on the SBA-15 surface affected their physicochemical properties and consequently exhibited a superior catalytic activity. Catalytic performances were conducted at optimum reaction conditions, as obtained by response surface methodology, in previous work [14]. We found an approach to the synthesis of propyl sulfonic acid functionalized SBA-15 ($PrSO_3H$-SBA-15) catalysts using a direct synthesis method, which offers a unique advantage over traditional grafting methods. In addition, the reusability of the prepared $PrSO_3H$ functionalized SBA-15 catalysts was tested over three consecutive runs.

2. Materials and methods

2.1. Materials

Tetraethyl orthosilicate (TEOS; 99 %), (3-mercaptopropyl)trimethoxysilane (MPTMS; 95 %), and PEG-PPG-PEG (Pluronic P123; Mw ~ 5800) were purchased from Sigma-Aldrich Chemical Co. Hydrogen peroxide [H_2O_2; 30 % (w/w)] was obtained from Merck & Co., Inc. Hydrochloric acid (HCl; 37 %) and methanol (AR grade) were procured from RCI Labscan Ltd. Sodium chloride (NaCl; 99.0–100.5 %) was purchased from Elago Enterprises Pty Ltd. Glycerol (99.5 %) and acetic acid (AR grade) were from Qrec Chemicals Co., Ltd.

2.2. Catalyst preparation

2.2.1. Synthesis of mesoporous SiO_2 (SBA-15)

The SBA-15 was synthesized according to the reported method [15] by dissolving 4 g of P123, 160 g of 2 M HCl, and 1.18 g of NaCl at 35 °C and stirring continuously for 2 h. Afterwards, TEOS (8.4 g) was dropped into the solution and stirred for 5 min. The solution was then aged in a water bath at 35 °C for 24 h followed by hydrothermal treatment in an oven at 100 °C for 24 h. The resultant white solid product was separated through vacuum filtration, washed with deionized water, dried at 80 °C overnight, and finally calcined at 500 °C for 12 h at a ramping rate of 1 °C /min.

2.2.2. Post synthesis of SA-SBA-15 (10%-P SA-SBA-15)

About 3 g of synthesized SBA-15 was dried in an oven at 120 °C for 4 h prior to being used in the post-synthesis method. Next, the dried SBA-15 was dispersed in a mixture of MPTMS and methanol and stirred for 30 min. The solution was then transferred to an autoclave and heated at 180 °C for 12 h. The white solid product was obtained by vacuum filtration, washed with excess methanol and dried at 100 °C overnight. The dried solid was labeled as SH-SBA-15, where SH represents the propyl thiol-functionalized SBA-15.

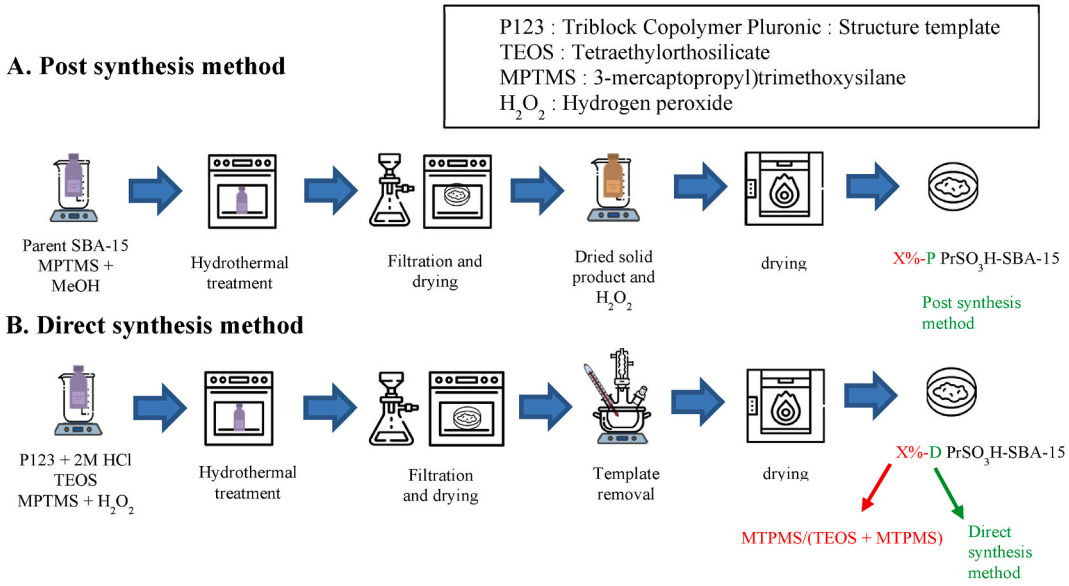

Scheme 1. Catalyst preparation procedure of $PrSO_3H$-SBA-15 catalysts.

Next, the thiol groups were oxidized to sulfonic acid groups by H_2O_2. Typically, SH-SBA-15 (3 g) was dissolved in 60 mL of a 1:1 (v/v) solution of 30 % (w/w) H_2O_2: deionized water at room temperature for 10 h. The solid products were recovered as described above. Finally, the dried catalyst was collected and denoted as 10%-P-SA-SBA-15, where 10 % represents the %mole of (MPTMS/(MPTMS + TEOS)), P refers to the post synthesis method and SA represents propyl sulfonic acid [16].

2.2.3. Direct synthesis of $PrSO_3H$ on mesoporous silica (X%-D SA-SBA-15)

The SA-SBA-15 was prepared by direct synthesis via co-condensation, as previously reported [17]. First, P123 (4 g) was dissolved in a 2 M HCl (125 mL) by stirring at room temperature for 2 h. Then, TEOS (6.83–8.11 g) was dropped into the solution and stirred at 40 °C for 45 min. Next, MPTMS (0.42–1.68 g) and 30 % (w/w) H_2O_2 were added into the solution and stirred at 40 °C for 20 h. Subsequently, the solution was heated in an oven at 100 °C for 24 h. After that, the white solid product was obtained through vacuum filtration and dried in air at room temperature overnight. The P123 scaffold was removed by solvent extraction (400 mL of ethanol/1.5 g of catalyst) at 78 °C for 24 h. Finally, the catalyst was dried in an oven at 120 °C for 9 h. The functionalized samples were denoted as X %-D-E/M SA-SBA-15, where X represents %mole of MPTMS/(MPTMS + TEOS), D represents direct synthesis method, and E or M represents washed with ethanol or methanol, respectively. The chemical composition, calculated in mole fraction units, was s: (1 - Y) TEOS: (Y) MPTMS: 18Y H_2O_2: 5.8 HCl: 0.017 P123: 165H_2O where Y was varied from 0.05 to 0.2 [18]. Procedures for SA-SBA-15 catalyst prepared by post synthesis and direct synthesis are shown in Scheme 1.

For the as-synthesized SA-SBA-15 catalysts, the procedures were similar to those mentioned above except without the washing step, with the obtained catalyst being denoted as 10%-SA-SBA-15.

2.3. Acetylation reaction

The catalytic performance test was conducted at the optimum condition found previously using RSM and selecting that with the best *p*-value and R-squared (R^2) value, and was determined to be a 1:9 glycerol: acetic acid molar feed ratio, and 115 °C for 8 h [14]. In a typical experiment, about 0.5 g of the prepared catalyst, 10.04 g of glycerol, and the desired amount of acetic acid were transferred into a 100-mL three-necked round-bottomed flask, which was immersed into a silicone oil bath at the desired reaction temperatures and continuously stirred under reflux. Reaction time was recorded after reaching the desired reaction temperature. The mixture was cooled to room temperature and filtered to collect the catalyst from the reaction solution using vacuum filtration. All measurements and experiments were performed in triplicate.

2.4. Reusability test

Reusability and regeneration of the 20%-D-E SA-SBA-15 catalyst was studied at 115 °C for 9 h using a 1:9 glycerol: acetic acid molar ratio. After the first run, the spent catalysts were filtered, washed with methanol, dried in an oven at 120 °C for 9 h, and denoted as RZ-MeOH (where Z refers to the number of recycle runs). The spent catalyst was regenerated by being reoxidized with 20 mL of 15 % (w/w) H_2O_2/g of spent catalyst for 4 h and subsequently washed, dried in an oven at 120 °C for 9 h, and denoted as RZ-H_2O_2, where Z refers to the recycle round. Reusability tests were sequentially tested under the optimum reaction conditions several times.

2.5. Product analysis

The glycerol and acetin products were analyzed by gas chromatography using an Agilent 7890B equipped with a HP-5 column (30 m × 0.32 mm id column, Agilent) and a flame ionization detector (FID). The reaction products (0.1 g) were diluted in 4.4 g ethanol and then 0.05 g butanol was added as an internal standard. Each sample (0.2 μL) was injected in a split mode with a split ratio of 6:1. The initial oven temperature was set at 70 °C and increased up to 180 °C and then to 250 °C at a heating rate of 5 °C/min and 10 °C/min, respectively, and the FID temperature was set at 310 °C. Then the glycerol conversion and acetin selectivity were calculated using the following equations:

$$\textit{Glycerol conversion}\ \ (X_{gly},\%) = \frac{\textit{initial mole of glycerol} - \textit{remained mole of glycerol}}{\textit{initial mole of glycerol}} \times 100$$

$$\textit{Selectivity}\ \ (S_i,\%) = \frac{\textit{mole of } i\ \textit{ product}}{\textit{total moles of products}} \times 100$$

The identification of chemical substances in liquid products was performed using nuclear magnetic resonance spectroscopy (NMR), sulfur analyzer, and Fourier transform infrared spectroscopy (FTIR). Product identification was performed on a Bruker Ultrashield 500 spectrometer (Magnet System 500 MHz). The product sample was mixed with sodium sulfate in order to trap the water. Each sample (150 μL) and DMSO-d6 (500 μL) was loaded in the NMR tube. The ^{13}C and ^{1}H NMR spectra of the prepared sample were recorded and TopSpin 4.1.4 software was employed to analyze the NMR spectra.

The sulfur contents in the liquid product was analyzed by a LECO, Truespec Sulfur analyzer. About 0.1 g of the liquid sample was transferred into the crucible boat and placed into the furnace at 1350 °C under oxygen. Then, the carrier gas carried the oxidized component (sulfur dioxide) to the separated column and detector, respectively.

The chemical functional groups of the liquid product were determined by FTIR analysis (Nicolet Nexus 670 Fourier transform infrared spectrometer with an iD7-ATR mode, Thermo Scientific, USA) using 64 scans and a spectral resolution of 4 cm^{-1}. The sample

was scanned in a range of 600–4000 cm^{-1}.

2.6. Kinetic analysis

A kinetic study of the acetylation reaction between glycerol and acetic acid was conducted over a temperature range of 85–115 °C using the 10%-D-E SA-SBA-15 catalyst [14]. According to previous work [19], the kinetic rate model was based on the Langmuir–Hinshelwood–Hougen–Watson (LHHW) model, with the kinetic rate equations expressed in Eqs. (1)–(4). The derivation of the kinetic rate equations are explained in the supplementary materials:

$$-r_{gly} = -\frac{dc_{gly}}{dt} = k_1 c_{gly} \tag{1}$$

$$r_{mono} = k_1 C_{gly} - k_2 C_{mono} \tag{2}$$

$$r_{di} = k_2 C_{mono} - k_3 C_{di} \tag{3}$$

$$r_{tri} = \frac{dc_{tri}}{dt} = k_3 c_{di} \tag{4}$$

The calculation of the kinetic rate constants (k_1, k_2, and k_3) was performed using the non-linear equation solver in polymath V.6 with the high R-squared (R^2) value. Each response has a zero value at the initial condition (time = 0).

2.7. Catalyst characterization

The physicochemical properties of the functionalized catalysts were investigated using nitrogen (N_2) adsorption–desorption, X-ray diffractometry (XRD), X-ray photoelectron spectroscopy (XPS), scanning electron microscopy (SEM), pyridine-adsorbed Fourier transform infrared spectroscopy (Py-FTIR), micro-Raman spectroscopy (Raman), and simultaneous thermal analysis (STA).

The crystallinity of the catalyst was determined by XRD analysis using a Rigaku, Smartlab X-ray diffractometer with CuKα radiation (λ = 1.541 Å) at 50 kV and 300 mA. The small-angle X-ray scattering patterns (SAXS) was recorded over a 2θ region of 0.5–3° at a step size and scanning rate of 0.02° and 0.5°/min, respectively. The specific surface area (S_{BET}) was calaulated using the Brunauer-Emmett-Teller (BET) method using a Quantachrome, Autosorb-IQ surface area analyzer. The samples were outgassed at 110 °C for 18 h under a high vacuum condition to remove volatile absorbents on the surface prior to analysis. The pore size distribution and total pore volume (V_p) were calculated using the Barrett–Joyner–Halenda (BJH) method from the desorption branch data. The d_p was obtained at the peak maximum of the BJH pore size distribution profile. The morphology of the catalysts was imaged by field emission (FE)-SEM using a Hitachi S-4800, Japan, operated at an accelerating voltage of 2 kV. The prepared sample was dried in an oven at 105 °C for 24 h.

The nature of the surface acidic sites was examined by Py-FTIR using pyridine as a molecular probe. A 30-mg sample was pressed into a 10 mm disc and then set into a quartz cell equipped with calcium fluoride windows. The cell was pretreated at 110 °C for 1 h under vacuum before being cooled to 50 °C, and then purged with pyridine gas for 30 min. The adsorbed catalyst was degassed at the same temperature. The FTIR spectrum of the adsorbed pyridine was then recorded on a Nicolet Nexus iS10 FTIR spectrometer (Thermo Fisher Scientific).

To measure the mass loss of P123, thermal gravimetric analysis was performed using STA with a NETZSCH STA 409 instrument. The mass loss of sample was monitored over a temperature range from 35 to 800 °C at a heating rate of 10 °C/min under N_2 at a flow rate of 20 mL/min.

The surface chemical compositions and chemistry of the catalysts were analyzed by XPS using a Kratos Axis Ultra DLD instrument equipped with monochromatic Al Kα radiation. All XPS spectra were analyzed using CasaXPS software (version 2.3.24PR1.0). Each C 1s spectrum was calibrated with the binding energy (BE) of 285 eV. The S 2p spectrum for a typical functionalized catalyst was used to confirm the presence of sulfonic acid groups on the surface of SBA-15.

The identification of functional groups was analyzed by micro-Raman spectroscopy using a XPloRA PLUS, Horiba. The solid-state laser had an excitation wavelength of 532 nm (laser power of 52.3 mW) with a grating of 1200 gr/mm. The samples were focused using a x50 long working distance. The micro-Raman spectra were collected over a range of 500–3600 cm^{-1}.

Table 2
Calculated rate constant at different reaction temperatures.

Temperature (°C)	k_1 (min^{-1})	k_2 (min^{-1})	k_3 (min^{-1})
85	1.67×10^{-2}	0.57×10^{-2}	0.17×10^{-2}
100	2.30×10^{-2}	0.81×10^{-2}	0.28×10^{-2}
115	3.15×10^{-2}	1.00×10^{-2}	0.30×10^{-2}

k_1, k_2, and k_3 are the rate constants (min^{-1}) for monoacetin, diacetin, and triacetin, respectively.
Data were obtained using the highest R^2 data set.

3. Results and discussion

3.1. Kinetic analysis

The derived temperature dependency of the rate constants is expressed in Table 2. Activation energies were determined from the slope of the linear plot between ln(k_i) and 1/T using the gas constant equal to 8.314 J/K•mol. The rate constants were k_1 (glycerol to monoacetin) > k_2 (monoacetin to diacetin) > k_3 (diacetin to triacetin). A higher temperature improved the acetin production corresponding to the Arrhenius equation. The high rate constant value for monoacetin production reflects the rapid monoacetin formation, whereas the low rate constant value for triacetin indicates the slow triacetin formation. In addition, the low activation energy for monoacetin formation from glycerol indicated how fast monoacetin formation was compared to those for diacetin from monoacetin and for triacetin from diacetin. This is in line with the rate constants obtained previously [19,20] using a CeO_2-ZrO_2 metal oxide catalyst and Amberlyst-15 catalyst at five and three different temperatures, respectively.

In this study, activation energies of 13.26, 21.66, and 35.01 kJ/mol at temperature range of 85–115 °C were obtained for the formation of monoacetin, diacetin, and triacetin, respectively; thus, the yield of triacetin is lower than mono- and diacetin in the reaction mixture. which were comparable to those reported previously of 7.2–26.6 kJ/mol using sulfated alumina catalyst [21] and 24.99–51.73 kJ/mol using heteropolyacid [22].

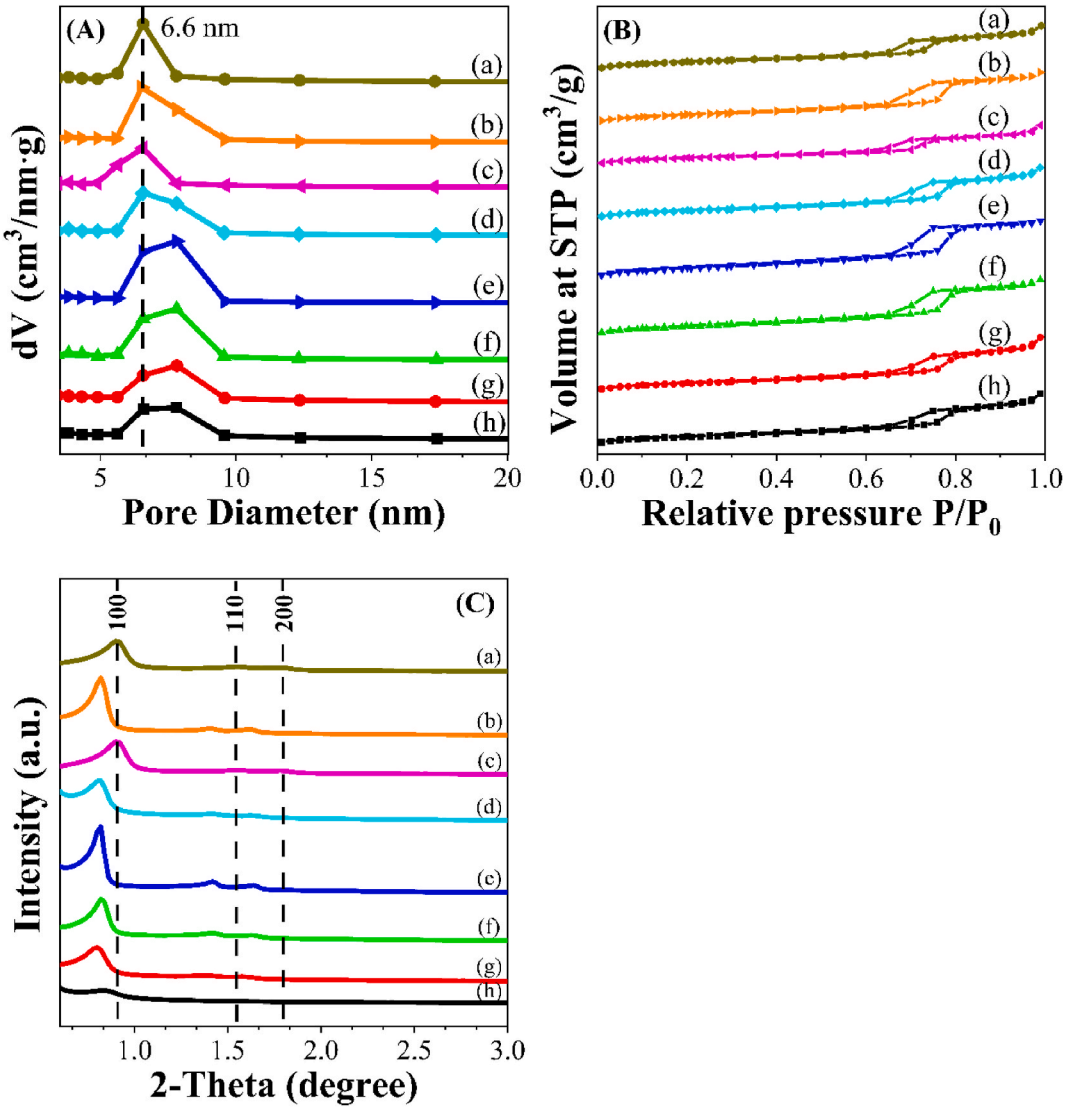

Fig. 1. Representative (A) pore size distribution, (B) N_2 adsorption–desorption isotherms, and (C) SAXS patterns of (a) SBA-15, (b) 10%-SA-SBA-15, (c) 10%-P SA-SBA-15, (d) 10%-D-M SA-SBA-15, (e) 5%-D-E SA-SBA-15, (f) 10%-D-E SA-SBA-15, (g) 15%-D-E SA-SBA-15, and (h) 20%-D-E SA-SBA-15.

3.2. Physicochemical properties of the SA-SBA-15 catalysts

Representative pore size distribution curves and N_2 adsorption-desorption isotherms of the prepared catalysts are presented in Fig. 1. The narrow pore size distribution (5–10 nm) was categorized as mesoporous materials following the IUPAC standard [23]. The hysteresis loop corresponded to the capillary condensation inside the pores of a mesoporous material and was in the P/P_0 range of 0.6–0.8 in Fig. 1(B), and categorized as a type IV isotherm [24]. The catalysts had a high S_{BET} and V_p (Table 3) in the range of 534–696 m^2/g and 0.9–1.3 cm^3/g, respectively. When the SA-SBA-15 catalysts were prepared by different synthesis methods or modified by different MPTMS loading levels and different washing solvents, it resulted in different physicochemical properties. The changes in these properties (S_{BET}, V_p, and d_p) shown in Table 3 are due to the presence of functional groups within the mesoporous structure of the support. The d_{100} values, unit cell parameter, and d_p of the prepared SA-SBA-15 were closer to those of the parent SBA-15, suggesting that the structure of SBA-15 was still preserved. However, a decrease in the d_{100} value and unit cell parameter was observed at higher SA loadings (20%-D-E SA-SBA-15).

Fig. 1(C) shows SAXS patterns of the prepared catalysts. The SBA-15 expressed three diffraction peaks at a 2θ of 0.9°, 1.6°, and 1.8° corresponding to the (100), (110), and (200) planes, respectively, which can be indexed on a two-dimensional hexagonal SBA-15 structure [25]. The higher peak intensity and a slight shift to a lower 2θ value indicated the presence of sulfonic groups inside the pores, which caused higher d-spacing and lattice parameter values.

Representative FE-SEM images of the SBA-15 modified with different loadings of sulfonic groups, as a mesoporous material, are demonstrated in Fig. 2. Rice-like shaped (5%-D-E SA-SBA-15, Fig. 2(a)) and rod-like shaped (10, 15, and 20%-D-E SA-SBA-15) morphologies were clearly observed in Fig. 2(b)–(d). Well uniformed hexagonal particles of 5%-D-E SA-SBA-15 were related to the high intensity of the diffraction peak in Fig. 1(C(e)). Then, the depletion of hexagonal shape and an increased non-uniform arrangement was observed, which is in line with the low intensity found in the XRD patterns. This is primarily due to the interaction between the sulfonic acid groups and the silica framework of SBA-15. In this direct synthesis method, this can potentially influence the formation of the silica structure and the subsequent distribution of sulfonic acid groups. Higher loadings of sulfonic acid groups can introduce defects or disrupt the regular structure of SBA-15. This can lead to changes in morphology, such as the formation of aggregates.

The organosilane incorporation on the SBA-15 catalyst was confirmed by XPS analysis, as summarized in Table 4. The quantitative analysis of the elemental content on the catalyst surface was performed using XPS in a wide scan mode. The amount of SA incorporated as sulfur on the surface indicated that the lowest amount was obtained by the catalyst prepared by post synthesis. The sulfur composition on the mesoporous SiO_2 surface varied from 2.43 to 5.87 at.%, depending on the synthesis method and organosilane loading level. A higher amount of sulfur was observed on SBA-15 with increasing amounts of incorporated SA.

3.2.1. Effect of solvent extraction

In the SBA-15 synthesis, surfactants are commonly used as the organic templates while thermal calcination is commonly used for template removal. In this present work, solvent extraction was used to remove the surfactant template of the SA-SBA-15 prepared by the direct method. Although it was reported that P123 extraction using methanol was more efficient than other solvents [26], it is interesting to compare the efficiency between methanol and ethanol. As clearly seen from TGA profiles in Fig. 3, the weight loss of water, P123, and -$PrSO_3H$ groups were centered at 120 °C, 260 °C, and 530 °C [27], respectively. The amount of P123 can be estimated by the weight loss between 120 and 340 °C. In the case of ethanol removal of P123, 2.94 % of the total mass was left compared to 5.06 % left by methanol, suggesting that ethanol was more efficient than methanol for removing the P123 (Table 5). Thus, the TGA revealed that 81 % of P123 was removed by ethanol compared to only 68 % by methanol. Note that the TGA results were consistent with the textural properties (Table 3). Using ethanol as the washing solvent resulted in a larger S_{BET}, V_p, and d_p of the prepared catalyst, indicating that a higher amount of the structure-directing agent (SDA) was removed. The S_{BET} (632 m^2/g) and total V_p (1.2 cm^3/g) of 10%-D-E SA-SBA-15 were much larger than those of 10%-D-M SA-SBA-15 (582 m^2/g and 1.0 cm^3/g, respectively), indicating the higher P123 removal efficiency by ethanol. In addition, a larger d_p (7.8 nm, Table 3) and higher crystallinity were obtained when using ethanol (10%-D-E SA-SBA-15) than when using methanol (6.6 nm). Although methanol is more polar than ethanol, the critical micelle

Table 3
Textural properties of the prepared catalysts.

Sample	S_{BET}[a] (m^2/g)	V_p (cm^3/g)	d_p[b] (nm)	Peak position (degree)	d_{100}[c] (nm)	a_0[d] (nm)	Wall thickness (nm)
SBA-15	695 ± 8.7	0.89	6.6	0.9	9.8	11.3	4.8
10%-SA-SBA-15	534 ± 7.2	0.97	6.5	0.8	10.8	12.5	6.0
10%-P-SA-SBA-15	556 ± 5.2	0.78	6.6	0.9	9.8	11.3	4.8
10%-D-M SA-SBA-15	582 ± 9.1	1.04	6.6	0.8	10.8	12.5	5.9
5%-D-E SA-SBA-15	696 ± 6.6	1.26	7.8	0.8	10.9	12.6	4.7
10%-D-E SA-SBA-15	632 ± 8.3	1.23	7.8	0.8	10.8	12.4	4.6
15%-D-E SA-SBA-15	560 ± 3.4	0.98	7.8	0.8	11.0	12.8	4.9
20%-D-E SA-SBA-15	541 ± 5.5	0.96	7.8	0.8	10.5	12.1	4.3

[a] Determined by the BET method.
[b] Obtained from the maximum of BJH method desorption pore size distribution.
[c] Calculated from the (100) plane reflection.
[d] Unit cell parameter (a_0) calculated from the position of the (100) diffraction.

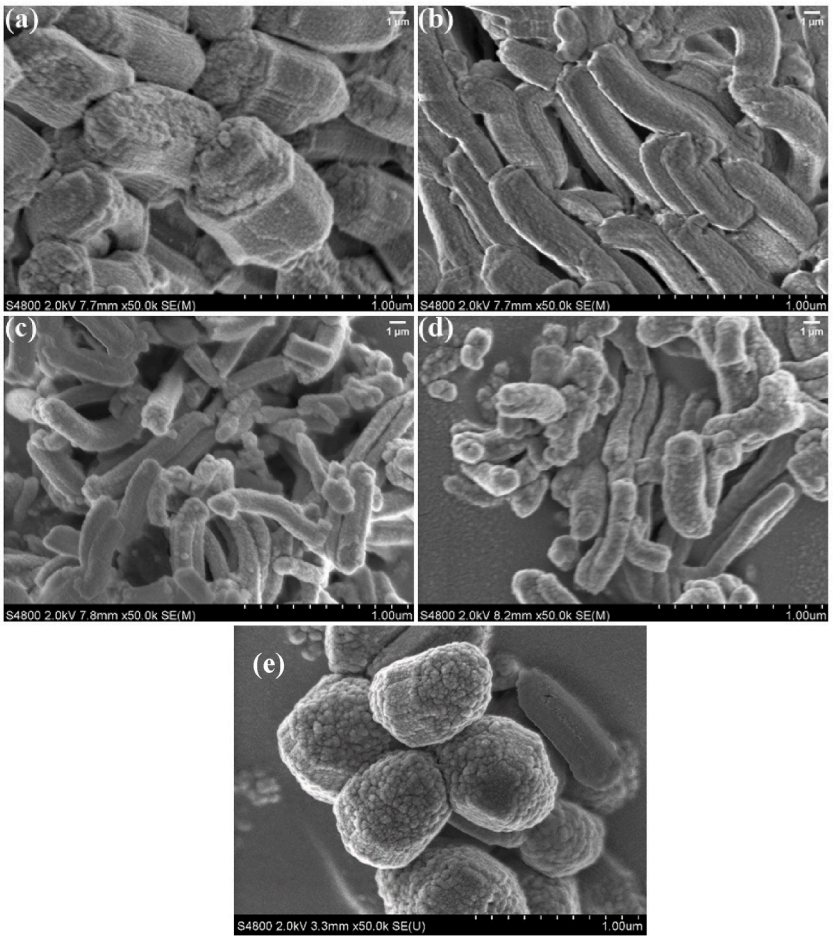

Fig. 2. Representative FE-SEM images (x50000 magnification) of the X%-D-E SA-SBA-15 catalysts with SA loading levels of (a) 5 %, (b) 10 %, (c) 15 %, (d) 20 %, and (e) SBA-15 support.

Table 4
Analysis of the sulfur content on the bulk surface and acidity property of the catalysts.

Catalyst	%Sulfur atoms on the surface[a]	% SO_3H from S 2p region[a]	Acidic property[b]				
			B acid sites (mmol/g)	L acid sites (mmol/g)	B/L	Total acidity (mmol/g)	Density of acidic sites (μmol/m^2)
10%-P SA-SBA-15	2.43	100.00	0.08	0.26	0.32	0.34	0.61
10%-D-M SA-SBA-15	n/a	n/a	0.18	0.18	1.01	0.37	0.64
5%-D-E SA-SBA-15	2.66	76.48	0.07	0.09	0.82	0.16	0.23
10%-D-E SA-SBA-15	3.39	85.17	0.25	0.21	1.16	0.46	0.73
15%-D-E SA-SBA-15	3.53	86.2	0.33	0.17	1.98	0.50	0.89
20%-D-E SA-SBA-15	5.87	100.00	0.45	0.07	6.28	0.53	0.98

Results were obtained by [a]XPS and [b]Py-FTIR analyses.
n/a: data is not available.

temperature of P123 in 1 M ethanol is slightly higher than that in 1 M methanol, resulting in a decreased level of micellar aggregation [28]. The higher P123 removal by methanol compared to other organic solvents was reported due to its high polarity [26,27]. We conclude from our results that ethanol is an effective solvent to remove the P123 templates and preserve a larger d_p and S_{BET} of the

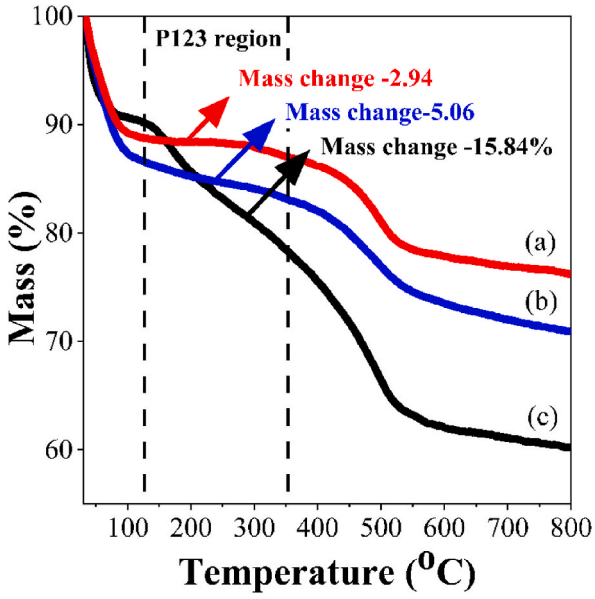

Fig. 3. Representative TGA profiles of (a) 10%-D-E SA-SBA-15, (b) 10%-D-M SA-SBA-15, and (c) 10%-SA-SBA-15.

Table 5
Comparison of P123 extraction from 10%-D SA-SBA-15 with different extraction solvents.

Sample	Solvent	Quantity	Duration	P123 wt%	P123 %removal
10%-SA-SBA-15	–	–	–	15.8	–
10%-D-M SA-SBA-15	MeOH	400 mL/1.5 g catalyst	24 h	5.1	68
10%-D-E SA-SBA-15	EtOH	400 mL/1.5 g catalyst	24 h	2.9	81

prepared catalyst.

3.2.2. Effect of the synthesis method

It is well known that the synthesis method significantly influences the physical properties of the obtained catalysts. Generally, a post synthesis method is used due to its high efficiency in the incorporation of the active species in the SBA-15 support. The parent SBA-15 is prepared first and then the sulfonic acid group is attached to the surface of the catalyst, rather than inserting into the silica structure in the direct synthesis [29]. Table 3 shows that using the post synthesis method gave catalysts with a lower S_{BET}, V_p, and d_p at the same sulfonic groups loading level (10%-P SA-SBA-15 and 10%-D-E SA-SBA-15). At a 10 % nominal mole of sulfonic acid functionalization, the (100) diffraction peak of 10%-D-E SA-SBA-15 was shifted towards a lower angle, indicating a larger interplanar distance (d_{100}) and unit cell parameter (a_0) [30,31]. The lower amount of sulfur on the surface of the catalyst prepared by post synthesis, as seen by XPS analysis, was due to the limited availability of reactive silanol groups on the surface of the SiO_2 material [32]. The data for direct synthesis in the present work agrees well with previous work [33] that direct synthesis leads to greater physicochemical properties (S_{BET}, V_p, and d_p) and promotes interaction between the active species and the support (the acidity via functionalization) than post synthesis. Thus, the direct synthesis of SA-SBA-15 was used in this study for further investigation.

3.2.3. Effect of the sulfonic groups loading level

The catalysts prepared by direct synthesis with different organosilane loadings were characterized. The S_{BET} and V_p of the catalyst obtained from a high incorporation of organosilane were diminished (Table 3). An enlarged wall thickness was evident, caused by the higher amount of anchored sulfonic acid groups on SBA-15, except for 20%-D-E SA-SBA-15 where mesoscopic disorder occurred. An increase in the amount of organosilane resulted in a lower intensity of diffraction peaks (Fig. 1(C)), owing to the disruption of micellar formation of P123 from the concentrated MPTMS [17]. In the same way, a higher MPTMS loading resulted in a greater wall thickness due to the deposition of sulfonic acid groups on the silica wall [34]. Likewise, a lower intensity of the diffraction peak was found when adding more MPTMS into the initial solution.

Increasing the MPTMS/(MPTMS + TEOS) ratio increased the length and decreased the width of the particles (Fig. 2), which was due to the charge repulsion between deprotonoted mercaptopropyl groups [35]. The morphology and support of mercapto-functionalized mesoporous silicas changing from short particles into whorled long rod-shaped particles has been reported previously [36]. It was speculated that the hydrophobic behavior of MPTMS produced an effect on the micellar shape of the surfactant that then directly affected the shape of the SiO2 particles. In the case of 20%-D-E SA-SBA-15, electrostatic forces play a role on the

particle shape, where a large amount of mercaptopropyl groups can produce the repulsive electrostatic force; therefore, the particle shape of the catalyst becomes more spherical with a mesoporous disorder demeanor, resulting in a larger particle size compared to 15%-D-E SA-SBA-15.

3.3. Acetylation of glycerol

The catalytic performance of various SA-SBA-15 catalysts in the acetylation of glycerol was performed with 5 wt% of catalyst at 115 °C for 8 h. The composition of acetin in the liquid product was composed of 1-monoacetin, 2-monoactin, 1,2-diacetin, 1,3-diacetin, and triacetin (Fig. S1), similar to other work [37]. The product selectivity depends strongly on the nature of the catalyst surface and strength of the active sites.

The glycerol conversion and products distribution obtained with the SA-SBA-15 catalysts are shown in Fig. 4, The presence of SA-SBA-15 in the acetylation reaction obviously improved the catalytic performance with the glycerol conversion level and triacetin selectivity being increased from 96.8 % and 13.3 % (blank test) to 100 % and 18.2–30.1 %, respectively. Comparing the synthesis method of 10%-P SA-SBA-15, a similar glycerol conversion level was observed (98.4–98.7 %) but the magnitude of triacetin selectivity was higher in the direct synthesis catalyst than that with the post synthesis catalyst. This is due to the limited sulfonic acid incorporation on the silanol surface in the post synthesis method. In our experiments, the large pore 10%-D-E SA-SBA-15 catalyst with pore diameter 7.8 nm exhibited higher triacetin than 10%-P SA-SBA-15 and 10%-D-M SA-SBA-15 catalysts with pore diameter of 6.6 nm, suggesting that the catalyst pore size is an important factor limiting triacetin formation with critical diameter of 1.0206 nm [10]. The larger pore sizes facilitate better diffusion and accessibility of reactants within the catalyst, thus enhancing the reaction efficiency and triacetin yield. Additionally, selectivity to triacetin was increased from 26.3 % to 30.1 % as the SA was increased from 5 % to 20 % in the SA-SBA-15 catalysts (D-G, Fig. 4), suggesting that the acidic sites are required for both the optimal glycerol conversion and triacetin selectivity. These catalysts showed a higher glycerol conversion level and triacetin selectivity compared to the previously reported 97 % and 23 %, respectively, from sulfonated bio-carbon based catalysts (starch as the carbon precursor) [38] at 110 °C with glycerol to acetic acid molar ratio of 1:6 within 2 h and 98.7 % and 27.5 %, respectively, from sulfated alumina catalysts [39] at 110 °C with glycerol to acetic acid molar ratio of 1:12 and catalyst amount of 0.36 g.

To be able to comprehend the capabilities of our prepared catalysts, the amount of Lewis (L) and Brønsted (B) acid sites in SA-SBA-15 was obtained from the FTIR spectra of adsorbed pyridine, as shown in Fig. 5. The deconvoluted results revealed that the bands at 1445, 1490, and 1546 cm^{-1} were clearly ascribed to L, L + B, and B acid sites, respectively. For SA-SBA-15, the Brønsted acid sites were mainly generated from anchored $PrSO_3H$- groups while the Lewis acid sites were created from siloxane bridge sites (Si-O-Si) on the SiO_2 surface [40]. The quantitative number of acid sites and the B/L ratio were calculated and are shown in Table 4.

Increasing the B/L ratio significantly enhanced triacetin selectivity (13.3–22.9 %) of the catalysts studied (blank test, Al-SA-SBA-15, and 10%-P SA-SBA-15; Fig. 6) due to the catalytic mechanism involving Brønsted acid sites. These sites facilitate the formation of a positively charged acylium ion intermediate, which attacks the hydroxyl groups on glycerol. The subsequent proton transfer and water removal drive the reaction forward, regenerating the Brønsted acid site, ultimately increasing triacetin yield [41]. For the D-E SA-SBA-15 catalyst series, the triacetin selectivity ranged from 26.3 to 30.1 %. At a B/L ratio of 6.28, the catalyst achieved a 100 % glycerol conversion level and 30.1 % triacetin selectivity, suggesting that the B/L ratio was directly related to the catalytic

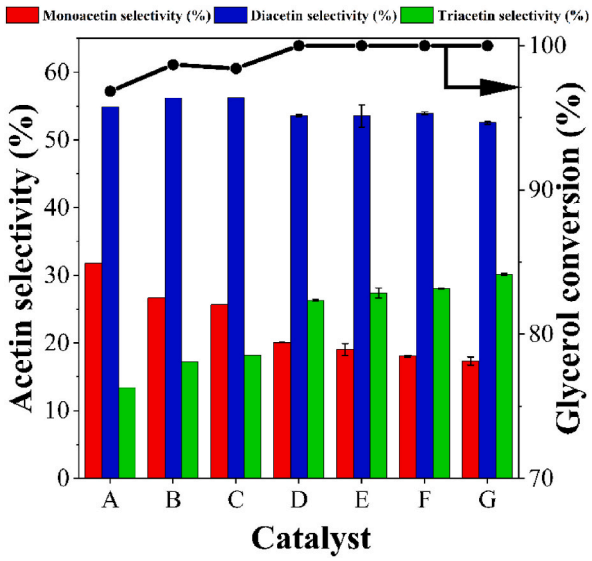

Fig. 4. Catalytic performances of the A) blank test, B) 10%-P SA-SBA-15, C) 10%-D-M SA-SBA-15, D) 5%-D-E SA-SBA-15, E) 10%-D-E SA-SBA-15, F) 15%-D-E SA-SBA-15, and G) 20%-D-E SA-SBA-15. Reaction conditions: catalyst loading of 0.5 g, molar feed ratio of 1:9 (Gly:AA), reaction temperature of 115 °C, and reaction time of 8 h. Data are shown as the mean ± standard deviation (SD).

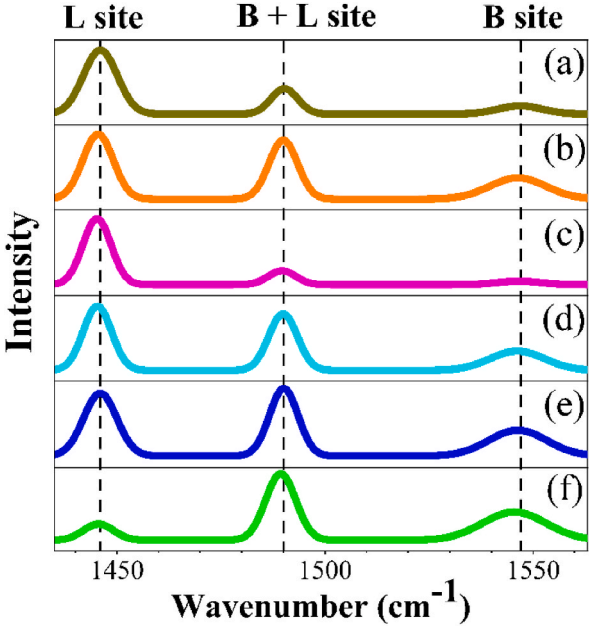

Fig. 5. Representative Py-FTIR spectra of (a) 10%-P SA-SBA-15, (b) 10%-D-M SA-SBA-15, (c) 5%-D-E SA-SBA-15, (d) 10%-D-E SA-SBA-15, (e) 15%-D-E SA-SBA-15, and (f) 20%-D-E SA-SBA-15.

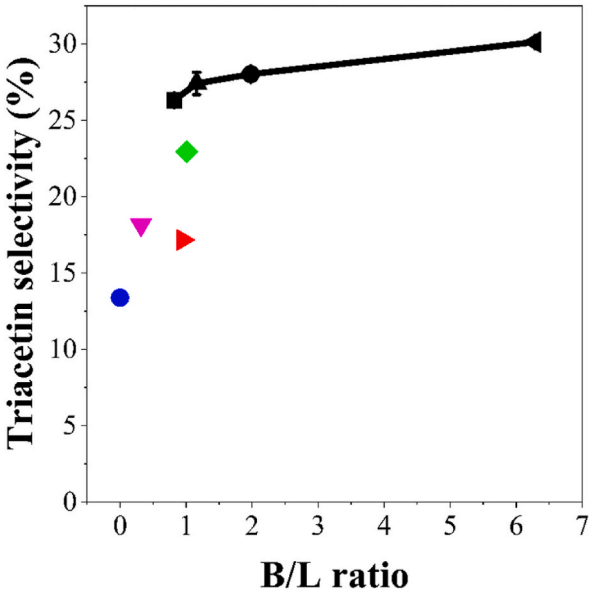

Fig. 6. Relationship between the B/L ratio and triacetin selectivity of the (●) blank (▶), Al-SA-SBA-15 (▼), 10%-P SA-SBA-15 (♦), 10%-D-M SA-SBA-15, (■) 5%-D-E SA-SBA-15, (▲) 10%-D-E SA-SBA-15, (●) 15%-D-E SA-SBA-15, and (◀) 20%-D-E SA-SBA-15. Data are shown as the mean ± standard deviation (SD). Reaction conditions: catalyst loading of 0.5 g, molar feed ratio of 1:9 (Gly:AA), reaction temperature of 115 °C, and reaction time of 8 h.

performance. A higher monoacetin selectivity was achieved (23.4–25.7 %) with the catalysts with a low B/L ratio (0.34–0.37). Therefore, the presence of Lewis acid sites can disrupt triacetin formation because it promotes monoacetin formation [12,42]. Interestingly, the influence of the solvent type (methanol and ethanol) for P123 extraction was noted, where the 10%-D-E SA-SBA-15 catalyst had a higher B/L ratio and triacetin selectivity than the 10%-D-M SA-SBA-15 catalyst at the same sulfonic acid loading level.

The acidic property of the samples was examined using the amount of pyridine that adsorbed on the catalyst active site. A higher SA amount gave more B acid sites (Table 4) because of the generation of sulfonic groups on the material surface. The B acid, L acid, total acidity, and density of acid sites were related to the catalytic performance and triacetin selectivity. It is interesting to note that the B/L

ratio and density of acid sites of the catalyst were correlated to the amount of SA in the initial mixture. However, for the large pore diameter (7.8 nm), 5%-D-E SA-SBA-15 with low acid site density exhibited higher triacetin selectivity than 10%-D-M SA-SBA-15 with high acid site density and small pore diameter (6.6 nm). It is interesting to note that both pore structure and surface acid site density significantly affect the acetin selectivity.

That sulfonic acid was successfully formed on the material surface supported from the S 2p XPS spectra (Fig. 7), which exhibited two major peaks at a BE of around 168 and 165 eV, corresponding to the sulfonic acid (-SO_3H) and thiol (-SH) groups, respectively [13]. Thus, the functionalization of -SO_3H groups was successfully anchored on the SBA-15 support, where the lower amount of organosilane displayed a higher amount of unconverted -SH groups due to the lower amount of H_2O_2 in the solution.

3.4. Reusability of the direct synthesized SA-SBA-15 catalyst

The reusability of the catalyst was evaluated using the 20%-D-E SA-SBA-15 catalyst because of its superior catalytic performance. After completion of the reaction, the catalyst was recovered by simple filtration, washed (to regenerate it), and reused in two or three consecutive reaction cycles. Comparison between two regeneration methods (methanol and H_2O_2) under the optimal reaction conditions was performed. The textural properties of the spent co-condensation $PrSO_3H$ SBA-15 catalysts regenerated by either acetone or H_2O_2 after use for furfural production from xylose both showed a decreased S_{BET} and V_p compared to the fresh catalyst due to the accumulation of byproduct (coke content) on the catalyst surface [43]. However, H_2O_2 regeneration exhibited more coke removal compared to acetone regeneration. Thus, H_2O_2 regeneration gave a better S_{BET} and V_p of the spent catalyst than acetone regeneration.

Examination of the textural properties of the spent catalysts in the present work revealed that the S_{BET}, V_p, and d_p were decreased, while the wall thickness (after regeneration) was increased compared to the fresh catalyst (Table 6). As expected, H_2O_2 regeneration resulted in better surface properties compared to methanol regeneration. The SAXS patterns of the spent 20%-D-E SA-SBA-15 catalysts did not change much after H_2O_2 oxidation compared to the fresh one (Fig. S2), suggesting that H_2O_2 had no significant effect on the structural properties of the SBA-15 support.

The surface composition of each type of catalyst was evaluated using XPS analysis (Fig. 8). For the methanol-regenerated catalysts, creation of -SH groups was observed after the catalyst was used and tended to increase after the first and second catalytic activity recycle passed, corresponding to the Raman spectra result. The Raman spectra of the fresh and spent 20%-D-E SA-SBA-15 catalysts are shown in Fig. S3. The position at 807, 1405, and 2924 cm^{-1} indicated the functional group of siloxane group, CH_2 deformation, and CH_2 stretching, respectively. Two sulfur functional groups, -SO_3H and -SH groups, were located at a peak position of 1045 and 2505 cm^{-1}, respectively [34,44]. The amount of -SH groups significantly increased from the fresh catalyst to the first and second regenerated catalysts, as evidenced by the increased intensity of the Raman shift at 2505 cm^{-1} and a decreased -SO_3H group peak at 1045 cm^{-1}. The formation of -SH groups from a reduction of SO_3H species is the most plausible deactivation cause. The spent catalyst after three consecutive cycles was regenerated by H_2O_2 (Fig. 8), where some of the lost SO_3H species were recovered, while the -SH groups decreased after the first (13.4 %) and second (9.78 %) catalytic activity recycles. A longer regeneration time (R3-H_2O_2) led to complete thiol group oxidation.

The catalytic activity of the spent catalysts, in terms of glycerol conversion and triacetin selectivity, are illustrated in Fig. 9. For

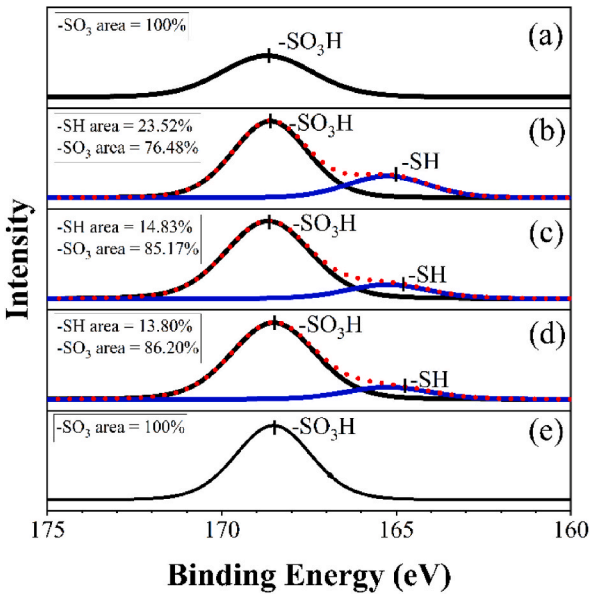

Fig. 7. Representative S 2p XPS spectra of the (a) 10%-P SA-SBA-15, (b) 5%-D-E SA-SBA-15, (c) 10%-D-E SA-SBA-15, (d) 15%-D-E SA-SBA-15, and (e) 20%-D-E SA-SBA-15.

Table 6
Textural properties of the spent catalysts.

Sample	S_{BET}[a] (m^2/g)	V_p (cm^3/g)	d_p[b] (nm)	Peak position (degree)	d_{100}[c] (nm)	a_0[d] (nm)	Wall thickness (nm)
20%-D-E SA-SBA-15	541 ± 5.5	1.0	7.8	0.8	10.5	12.1	4.3
R1-MeOH	470 ± 4.1	0.6	3.8	0.8	10.9	12.6	8.8
R2-MeOH	431 ± 2.3	0.5	3.8	0.8	11.2	12.9	9.1
R1-H_2O_2	578 ± 3.0	0.6	3.9	0.8	10.4	12.0	8.1
R2-H_2O_2	617 ± 5.8	0.7	3.8	0.9	10.3	11.9	8.0
R3-H_2O_2	409 ± 3.4	0.5	3.8	0.8	10.5	12.1	8.3

[a] Determined by the BET method.
[b] Obtained from the maximum of BJH method desorption pore size distribution.
[c] Calculated from the (100) plane reflection.
[d] Unit cell parameter (a_0) calculated from the position of the (100) diffraction.

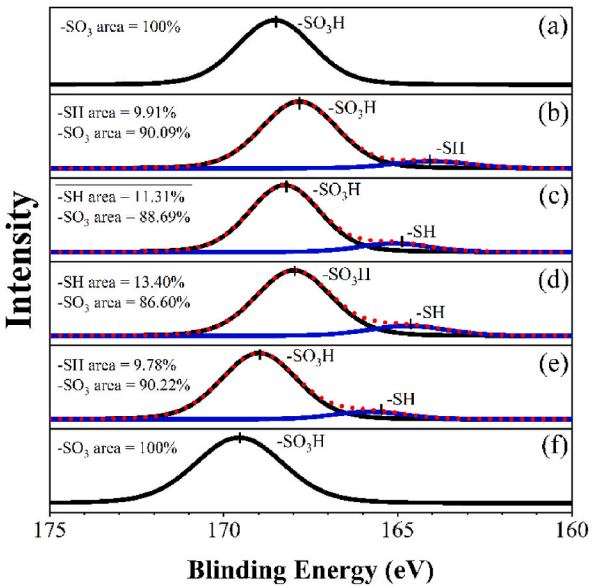

Fig. 8. (A) Representative S 2p XPS spectra of the (a) 20%-D-E SA-SBA-15, (b) R1-MeOH, (c) R2-MeOH, (d) R1-H_2O_2, (e) R2-H_2O_2, and (f) R3-H_2O_2.

methanol regeneration, after the first regeneration the catalyst retained a 100 % glycerol conversion level and a high triacetin selectivity of 26.2 %; however, after the second regeneration the glycerol conversion level was slightly reduced to 98.6 % with a substantially decreased triacetin selectivity to 17.7 % (Table S1). For the H_2O_2-regenerated catalysts, they exhibited the same trend in catalytic activity as the methanol-regenerated catalysts, but after the third H_2O_2-regeneration, which was performed for a longer time (24 h), the catalytic performance was slightly increased compared to after two regenerations. Thus, a longer regeneration time can only minimally improve the performance of the catalyst.

According to the catalytic activity and characterization results of the spent catalysts, it can be concluded that deterioration of functionalized groups on the catalyst's surface leads to the loss of catalytic performance. This was due to the reduction of active -SO_3H groups into -SH groups, resulting in weak acid sites [45] and a decreased S_{BET}, V_p, and d_p due to chemical deposition inside the catalyst pore. A similar trend of catalytic activity for spent catalysts has been reported previously [46]. A sulfated alumina catalyst was tested in the acetylation of glycerol over three consecutive runs with the spent catalyst being regenerated with acetone. The triacetin selectivity was clearly decreased in the second regenerated catalyst, decreasing by 26.7 % from that for the fresh catalyst, but without any change in the glycerol conversion level. In this case, deactivation of the catalyst was due to leaching out of the active species of the catalyst. The reusability of a sulfonic acid-functionalized carbon sphere (CS) catalyst revealed similar patterns of decreasing glycerol conversion and, especially, triacetin selectivity with increasing cycles of use. For the CS catalyst, glycerol conversion was minimally decreased from 98 % to 95 % for the first to fourth reaction cycle, respectively. However, after four reaction cycles the triacetin selectivity was reduced by 59.1 % compared to first reaction, which was due to leaching out of the sulfur content [47].

In addition, in order to monitor the leached species in the mixture, the liquid sample was evaluated by FTIR and sulfur analyses. The FTIR spectra of the obtained liquid products (Fig. S4) from the reusability test confirmed that there was no difference in the functional group and peak intensity of the liquid product from the fresh and reused catalysts, where the observed peaks at 3008, 1707, 1386, 1225, and 1048 cm^{-1} were attributed to O-H stretching, C=O stretching, C-O-H, C-C(O)-C stretching, and O-H bending, respectively [48]. In addition, the sulfur analyzer results (Table S2) demonstrated that the small amount of detected sulfur in the product liquid was

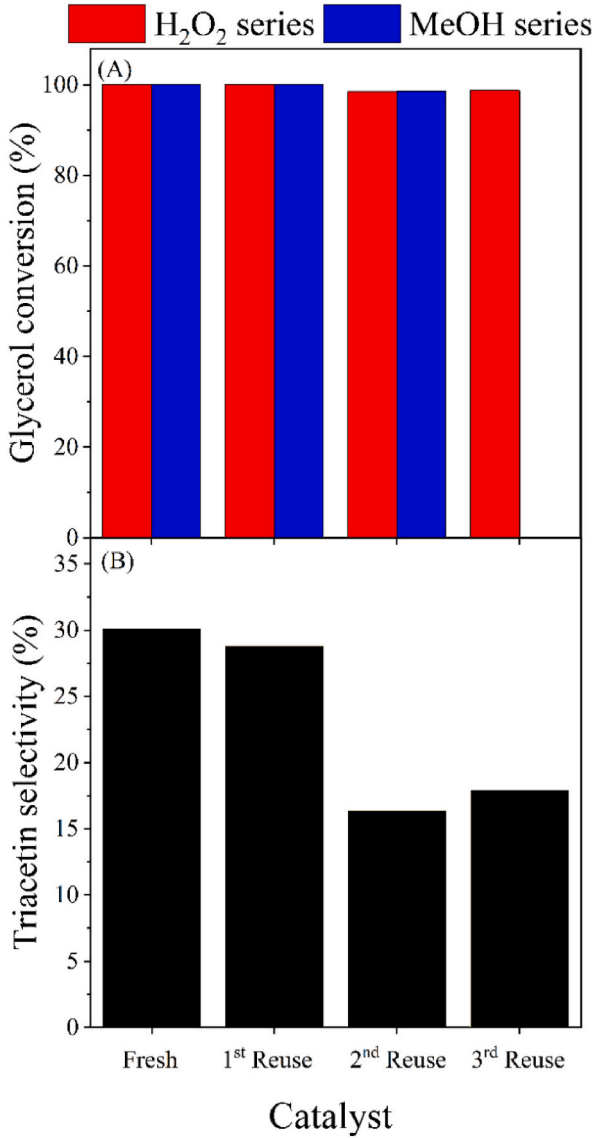

Fig. 9. Reusability of the catalysts in terms of the (A) glycerol conversion level and (B) triacetin selectivity of H_2O_2-regenerated catalysts at different recycle rounds. Reaction conditions: catalyst loading of 0.5 g, molar feed ratio of 1:9 (Gly:AA), reaction temperature of 115 °C, and reaction time of 8 h.

considered as an insignificant loss. Therefore, the sulfur species on the functionalized catalyst was probably attached on the catalyst's surface without leaching into the liquid product.

4. Conclusions

This study revealed the catalytic performances of SA-SBA-15 catalysts prepared by direct synthesis in the glycerol acetylation reaction and its reusability. During catalyst preparation, higher levels of P123 were effectively removed by ethanol washing than methanol washing in the direct synthesis approach. Decreasing the amount of aggregation of micelles of the SDA (lower residual P123 levels) affected the properties and structure of catalyst. The SA-SBA-15 prepared by direct synthesis expressed a higher level of organosilane anchored on the silica surface, resulting in a higher amount of acid sites on the SBA-15 surface than that prepared by post synthesis. The presence of Brønsted acid sites and large pore structure clearly enhanced the catalytic performance. Increasing the SA loading increased the amount of B/L sites, which then enhanced both the glycerol conversion level (100 %) and triacetin selectivity (30.1 %). Reduction of -SO_3H groups into -SH groups and changes in the textural properties of the catalyst both significantly affected the reusability of the catalyst.

CRediT authorship contribution statement

Panida Sriratchatchawan: Writing – original draft, Methodology, Investigation, Conceptualization. **Srisin Eaimsumang:** Formal analysis. **Siwaporn Meejoo Smith:** Supervision. **Supakorn Boonyuen:** Supervision. **Chawalit Ngamcharussrivichai:** Supervision, Project administration. **Apanee Luengnaruemitchai:** Writing – review & editing, Project administration, Conceptualization.

Data availability statement

Data will be made available on request.

Ethics declaration

This manuscript is original work and has not been submitted for publication elsewhere. All sources of information have been acknowledged. The authors have obtained necessary permissions to use copyrighted material. This article does not contain any studies involving human or animal subjects.

Declaration of competing interest

The authors declare the following financial interests/personal relationships which may be considered as potential competing interests: Apanee Luengnaruemitchai reports financial support was provided by National Science, Research and Innovation Fund (NSRF), Thailand. If there are other authors, they declare that they have no known competing financial interests or personal relationships that could have appeared to influence the work reported in this paper.

Acknowledgements

The authors are grateful to the Petroleum and Petrochemical College. This research was funded by the Thailand Science Research and Innovation Fund Chulalongkorn University (CU_FRB640001_01_23_2) and (BCG66630027) and the National Science, Research and Innovation Fund (NSRF) via the Program Management Unit for Human Resources & Institutional Development, Research and Innovation (B05F640151), Thailand.

Appendix A. Supplementary data

Supplementary data to this article can be found online at https://doi.org/10.1016/j.heliyon.2024.e41044.

References

[1] T.U. Nations, COP26: together for our planet. https://www.un.org/en/climatechange/cop26, 2021. (Accessed 22 November 2022).
[2] M.H. Hassan, M.A. Kalam, An overview of biofuel as a renewable energy source: development and challenges, Procedia Eng. 56 (2013) 39–53, https://doi.org/10.1016/j.proeng.2013.03.087.
[3] J. Van Gerpen, B. Shanks, R. Pruszko, D. Clements, G. Knothe, Biodiesel Production Technology, Subcontractor Report to U.S. Department of Energy, 2004. (Accessed 22 November 2022).
[4] K. Hanaki, J. Portugal-Pereira, in: K. Takeuchi, H. Shiroyama, O. Saito, M. Matsuura (Eds.), The Effect of Biofuel Production on Greenhouse Gas Emission Reductions, Springer Japan, Tokyo, 2018, pp. 53–71.
[5] A.L. Chun Minh, S.P. Samudrala, S. Bhattacharya, Valorisation of glycerol through catalytic hydrogenolysis routes for sustainable production of value-added C_3 chemicals: current and future trends, Sustain. Energy Fuels 6 (2022) 596–639, https://doi.org/10.1039/D1SE01333E.
[6] X. Liao, Y. Zhu, S.-G. Wang, H. Chen, Y. Li, Theoretical elucidation of acetylating glycerol with acetic acid and acetic anhydride, Appl. Catal., B 94 (2010) 64–70, https://doi.org/10.1016/j.apcatb.2009.10.021.
[7] T. Laino, C. Tuma, P. Moor, E. Martin, S. Stolz, A. Curioni, Mechanisms of Propylene glycol and triacetin pyrolysis, J. Phys. Chem. A 116 (2012) 4602–4609, https://doi.org/10.1021/jp300997d.
[8] P.T. George, E.K. John. Bonding plasticizers for cigarette filters of cellulose acetate fibers, The United States US3393684A, 1968.
[9] J.D. Puche, Use of Glycerine Tri-acetate as Additive of Biodiesel Fuel Compositions, European Patent EP1331260B1, 2008.
[10] L.J. Konwar, P. Mäki-Arvela, P. Begum, N. Kumar, A.J. Thakur, J.-P. Mikkola, R.C. Deka, D. Deka, Shape selectivity and acidity effects in glycerol acetylation with acetic anhydride: selective synthesis of triacetin over Y-zeolite and sulfonated mesoporous carbons, J. Catal. 329 (2015) 237–247, https://doi.org/10.1016/j.jcat.2015.05.021.
[11] M. Popova, H. Lazarova, Á. Szegedi, R.M. Mihályi, M. Rangus, B. Likozar, V.D.B.C. Dasireddy, Renewable glycerol esterification over sulfonic-modified mesoporous silicas, J. Serbian Chem. Soc. 83 (1) (2018) 39–50, https://doi.org/10.2298/JSC170306071P.
[12] G.A. Bedogni, M.D. Acevedo, F. Aguzín, N.B. Okulik, C.L. Padró, Synthesis of bioadditives of fuels from biodiesel-derived glycerol by esterification with acetic acid on solid catalysts, Environ. Technol. 39 (2018) 1955–1966, https://doi.org/10.1080/09593330.2017.1345986.
[13] M.L. Testa, V. La Parola, L.F. Liotta, A.M. Venezia, Screening of different solid acid catalysts for glycerol acetylation, J. Mol. Catal. A: Chem. 367 (2013) 69–76, https://doi.org/10.1016/j.molcata.2012.10.027.
[14] P. Sriratchatchawan, S. Eaimsumang, A. Luengnaruemitchai, Optimization of reaction conditions for acetylation of glycerol and acetic acid using statistical method. In the 28th PPC Symposium on Petroleum, Petrochemicals, and Polymers and the 13th Research Symposium on Petrochemical and Materials Technology /the Petroleum and Petrochemical College, 2022, pp. 37–43. Thailand.
[15] P. Tosuwan, S.-Y. Chen, H. Tateno, T. Mochizuki, A. Luengnaruemitchai, An aluminum-grafted SBA-15-catalyzed conversion of glucose to 5-hydroxymethylfurfural, Catal. Commun. 170 (2022) 106488, https://doi.org/10.1016/j.catcom.2022.106488.

[16] C. Thunyaratchatanon, W. Sinsakullert, A. Luengnaruemitchai, K. Faungnawakij, 5-Hydroxymethylfurfural production from hexose sugars using adjustable acid- and base-functionalized mesoporous SBA-15 catalysts in aqueous media, Biomass Convers. Biorefinery 11 (2021) 1733–1747, https://doi.org/10.1007/s13399-019-00553-8.

[17] D. Margolese, J.A. Melero, S.C. Christiansen, B.F. Chmelka, G.D. Stucky, Direct syntheses of ordered SBA-15 mesoporous silica containing sulfonic acid groups, Chem. Mater. 12 (2000) 2448–2459, https://doi.org/10.1021/cm0010304.

[18] X. Wang, S. Cheng, J.C.C. Chan, Propylsulfonic acid-functionalized mesoporous silica synthesized by in situ oxidation of thiol groups under template-free condition, J. Phys. Chem. C 111 (2007) 2156–2164, https://doi.org/10.1021/jp066924b.

[19] L. Zhou, T.-H. Nguyen, A.A. Adesina, The acetylation of glycerol over amberlyst-15: kinetic and product distribution, Fuel Process. Technol. 104 (2012) 310–318, https://doi.org/10.1016/j.fuproc.2012.06.001.

[20] R.M. Kulkarni, P.J. Britto, A. Narula, S. Saqline, D. Anand, C. Bhagyalakshmi, R.N. Herle, Kinetic studies on the synthesis of fuel additives from glycerol using CeO_2–ZrO_2 metal oxide catalyst, Biofuel Res. J. 7 (2020) 1100–1101, https://doi.org/10.18331/BRJ2020.7.1.2, 108.

[21] A. Pankajakshan, S.M. Pudi, P. Biswas, Acetylation of glycerol over highly stable and active sulfated alumina catalyst: reaction mechanism, Kinetic modeling and estimation of kinetic parameters, Int. J. Chem. Kinet. 50 (2018) 98–111, https://doi.org/10.1002/kin.21144.

[22] S. Veluturla, A. Narula, S.R.D, S.P. Shetty, Kinetic study of synthesis of bio-fuel additives from glycerol using a hetropolyacid, Resour.-Efficient Technol. 3 (2017) 337–341, https://doi.org/10.1016/j.reffit.2017.02.005.

[23] K. Ariga, A. Vinu, Y. Yamauchi, Q. Ji, J. Hill, Nanoarchitectonics for mesoporous materials, Bull. Chem. Soc. Jpn. 85 (2012) 1–32, https://doi.org/10.1246/bcsj.20110162.

[24] M. Thommes, K. Kaneko, A.V. Neimark, J.P. Olivier, F. Rodriguez-Reinoso, J. Rouquerol, K.S.W. Sing, Physisorption of gases, with special reference to the evaluation of surface area and pore size distribution (IUPAC technical report), Pure Appl. Chem. 87 (2015) 1051–1069, https://doi.org/10.1515/pac-2014-1117.

[25] H.I. Lee, J.H. Kim, G.D. Stucky, Y. Shi, C. Pak, J.M. Kim, Morphology-selective synthesis of mesoporous SBA-15 particles over micrometer, submicrometer and nanometer scales, J. Mater. Chem. 20 (2010) 8483–8487, https://doi.org/10.1039/C0JM00820F.

[26] S.G. de Ávila, L.C.C. Silva, J.R. Matos, Optimisation of SBA-15 properties using Soxhlet solvent extraction for template removal, Micropor Mesopor Mat 234 (2016) 277–286, https://doi.org/10.1016/j.micromeso.2016.07.027.

[27] C. Pirez, K. Wilson, A.F. Lee, An energy-efficient route to the rapid synthesis of organically-modified SBA-15 via ultrasonic template removal, Green Chem. 16 (2014) 197–202, https://doi.org/10.1039/C3GC40474A.

[28] B. Bharatiya, C. Guo, J.H. Ma, P.A. Hassan, P. Bahadur, Aggregation and clouding behavior of aqueous solution of EO–PO block copolymer in presence of n-alkanols, Eur. Polym 43 (2007) 1883–1891, https://doi.org/10.1016/j.eurpolymj.2007.02.010.

[29] M. Moritz, M. Geszke-Moritz, Mesoporous materials as multifunctional tools in biosciences: principles and applications, Mater. Sci. Eng. C. 49 (2015) 114–151, https://doi.org/10.1016/j.msec.2014.12.079.

[30] B. Erdem, S. Erdem, R.M. Öksüzoğlu, Catalytic applications of large pore sulfonic acid-functionalized SBA-15 mesoporous silica for esterification, Open Chem. 16 (2018) 1233–1241, https://doi.org/10.1515/chem-2018-0132.

[31] O.C. Gobin, Y. Wan, D. Zhao, F. Kleitz, S. Kaliaguine, Mesostructured silica SBA-16 with tailored intrawall porosity part 1: synthesis and characterization, J. Phys. Chem. C 111 (2007) 3053–3058, https://doi.org/10.1021/jp0635765.

[32] J.A. Melero, R. van Grieken, G. Morales, Advances in the synthesis and catalytic applications of organosulfonic-functionalized mesostructured materials, Chem. Rev. 106 (2006) 3790–3812, https://doi.org/10.1021/cr050994h.

[33] P.F. Siril, N.R. Shiju, D.R. Brown, K. Wilson, Optimising catalytic properties of supported sulfonic acid catalysts, Appl. Catal. 364 (2009) 95–100, https://doi.org/10.1016/j.apcata.2009.05.032.

[34] A.S. Cattaneo, C. Ferrara, D.C. Villa, S. Angioni, C. Milanese, D. Capsoni, S. Grandi, P. Mustarelli, V. Allodi, G. Mariotto, S. Brutti, E. Quartarone, SBA-15 mesoporous silica highly functionalized with propylsulfonic pendants: a thorough physico-chemical characterization, Micropor. Mesopor. Mat. 219 (2016) 219–229, https://doi.org/10.1016/J.MICROMESO.2015.08.011.

[35] S. Sadasivan, D. Khushalani, S. Mann, Synthesis and shape modification of organo-functionalised silica nanoparticles with ordered mesostructured interiors, J. Mater. Chem. 13 (2003) 1023–1029, https://doi.org/10.1039/B300851G.

[36] X. Du, J. He, Elaborate control over the morphology and structure of mercapto-functionalized mesoporous silicas as multipurpose carriers, Dalton Trans. 39 (2010) 9063–9072, https://doi.org/10.1039/C0DT00194E.

[37] A. Casas, M.J. Ramos, Á. Pérez, A. Simón, C. Lucas-Torres, A. Moreno, Rapid quantitative determination by 13C NMR of the composition of acetylglycerol mixtures as byproduct in biodiesel synthesis, Fuel 92 (2012) 180–186, https://doi.org/10.1016/j.fuel.2011.06.061.

[38] A. Malaika, K. Ptaszyńska, M. Kozłowski, Conversion of renewable feedstock to bio-carbons dedicated for the production of green fuel additives from glycerol, Fuel 288 (2021) 119609, https://doi.org/10.1016/j.fuel.2020.119609.

[39] A. P, S.M. Pudi, P. Biswas, Acetylation of glycerol over sulfated alumina: reaction parameter study and optimization using response surface methodology, Energy Fuels 30 (2016) 584–593, https://doi.org/10.1021/acs.energyfuels.5b01901.

[40] D.A. Cabrera-Munguia, H. González, E. Tututi-Ríos, A. Gutiérrez-Alejandre, J.L. Rico, Acid properties of M-SBA-15 and M-SBA-15-SO_3H (M = Al, Ti) materials and their role on esterification of oleic acid, J. Mater. Res. 33 (2018) 3634–3645, https://doi.org/10.1557/jmr.2018.374.

[41] U.I. Nda-Umar, I.B. Ramli, E.N. Muhamad, N. Azri, U.F. Amadi, Y.H. Taufiq-Yap, Influence of heterogeneous catalysts and reaction parameters on the acetylation of glycerol to acetin: a review, Appl. Sci. 10 (2020) 7155, https://doi.org/10.3390/app10207155.

[42] C. Gonzalez-Arellano, R.A.D. Arancon, R. Luque, Al-SBA-15 catalysed cross-esterification and acetalisation of biomass-derived platform chemicals, Green Chem. 16 (2014) 4985–4993, https://doi.org/10.1039/C4GC01105H.

[43] X. Shi, Y. Wu, H. Yi, G. Rui, P. Li, M. Yang, G. Wang, Selective preparation of furfural from xylose over sulfonic acid functionalized mesoporous SBA-15 materials, Energies 4 (2011) 669–684, https://doi.org/10.3390/en4040669.

[44] M. Mazilu, A.C. De Luca, A. Riches, C. Herrington, K. Dholakia, Optimal algorithm for fluorescence suppression of modulated Raman spectroscopy, Opt Express 18 (2010) 11382–11395, https://doi.org/10.1364/OE.18.011382.

[45] R.J. Ouellette, J.D. Rawn, in: R.J. Ouellette, J.D. Rawn (Eds.), Alcohols and Phenols, Elsevier, Boston, 2015, pp. 209–238.

[46] F.B. Ferreira, M.J. da Silva, FdÁ. Rodrigues, W.L. da Silva Faria, Sulfated-alumina-catalyzed triacetin synthesis: an optimization study of glycerol esterification, Ind. Eng. Chem. Res. 61 (2022) 4235–4243, https://doi.org/10.1021/acs.iecr.1c04782.

[47] A. Malaika, M. Kozłowski, Glycerol conversion towards valuable fuel blending compounds with the assistance of SO_3H-functionalized carbon xerogels and spheres, Fuel Process. Technol. 184 (2019) 19–26, https://doi.org/10.1016/j.fuproc.2018.11.006.

[48] M. Danish, M. Mumtaz, M. Fakhar, T.D.U. Rashid, Response surface methodology based optimized purification of the residual glycerol from biodiesel production process, Chiang Mai J. Sci. 44 (2017) 1570–1582.